Nanoscale Res Lett (2009) 4:858–864
DOI 10.1007/s11671-009-9334-6

NANO EXPRESS

Assessment of the In Vivo Toxicity of Gold Nanoparticles

Yu-Shiun Chen · Yao-Ching Hung · Ian Liau · G. Steve Huang

Received: 31 March 2009 / Accepted: 24 April 2009 / Published online: 8 May 2009

Abstract The environmental impact of nanoparticles is evident; however, their toxicity due to their nanosize is rarely discussed. Gold nanoparticles (GNPs) may serve as a promising model to address the size-dependent biological response to nanoparticles because they show good biocompatibility and their size can be controlled with great precision during their chemical synthesis. Naked GNPs ranging from 3 to 100 nm were injected intraperitoneally into BALB/C mice at a dose of 8 mg/kg/week. GNPs of 3, 5, 50, and 100 nm did not show harmful effects; however, GNPs ranging from 8 to 37 nm induced severe sickness in mice. Mice injected with GNPs in this range showed fatigue, loss of appetite, change of fur color, and weight loss. Starting from day 14, mice in this group exhibited a camel-like back and crooked spine. The majority of mice in these groups died within 21 days. Injection of 5 and 3 nm GNPs, however, did not induce sickness or lethality in mice. Pathological examination of the major organs of the mice in the diseased groups indicated an increase of Kupffer cells in the liver, loss of structural integrity in the lungs, and diffusion of white pulp in the spleen. The pathological abnormality was associated with the presence of gold particles at the diseased sites, which were verified by ex vivo Coherent anti-Stoke Raman scattering microscopy. Modifying the surface of the GNPs by incorporating immunogenic peptides ameliorated their toxicity. This reduction in the toxicity is associated with an increase in the ability to induce antibody response. The toxicity of GNPs may be a fundamental determinant of the environmental toxicity of nanoparticles.

Keywords Gold nanoparticles · Nanotoxicity · Immunogenicity · Mice · Toxicity

Y.-S. Chen · G. S. Huang (✉)
Institute of Nanotechnology, National Chiao Tung University, Hsinchu, Taiwan, ROC
e-mail: gstevehuang@mail.nctu.edu.tw

Y.-S. Chen
Department of Material Science and Engineering, National Chiao Tung University, Hsinchu, Taiwan, ROC

Y.-C. Hung
Section of Gynecologic Oncology, Department of Obstetrics and Gynecology, China Medical University and Hospital, 91 Hsueh Shih Rd., Taichung 404, Taiwan, ROC

I. Liau
Department of Applied Chemistry, National Chiao Tung University, Hsinchu, Taiwan, ROC

Introduction

The environmental impact of nanoparticles is evident; however, their nanotoxicity due to the reduction in size to nanoscale is rarely discussed. Gold nanoparticles (GNPs) may serve as a promising model to address this size-dependent toxicity, since gold is extraordinarily biocompatible.

Recently, the increased toxicity of nanoparticles due to their tiny physical dimensions has been widely recognized [1–3]. Carbon black is nontoxic; however, carbon nanotubes and fullerene are highly toxic when inhaled into the lungs [4–6]. Similarly, enhanced toxicity of titanium oxide nanoparticles has been reported [7, 8] and titanium oxide nanoparticles have been shown to induce oxidative stress in bacteria [9]. A large number of non-toxic bulk materials become poisonous when their size is reduced to nanoscale. However, the toxicity may be due more to the unique surface chemistry of the individual nanoparticle and less to the reduction in size per se.

The toxicity of GNPs has been investigated at the cellular level. GNPs enter cells in a size- and shape-dependent manner [10, 11]. Uptake of GNPs reaches a maximum when the size nears 50 nm and when the aspect ratio approaches unity. The transport efficiency reaches a plateau 30 min after incubation. The uptake of GNPs is consistent with receptor-mediated endocytosis. Nevertheless, most GNPs can enter cells efficiently, and most studies indicate that they are nearly harmless to cultured cells [12–15].

We have previously shown that GNPs are capable of inducing an antibody response in mice, which indicates that factors other than cytotoxicity may be involved and complicates in vivo application of GNPs [16]. The current study is based on the hypothesis that the reduction in size per se may make harmless GNPs toxic to live animals.

Materials and Methods

Materials

$HAuCl_4$, sodium citrate, $NaBH_4$, HCl, HNO_3, H_2SO_4, H_2O_2, and other chemicals of analytical grade were purchased from Sigma-Aldrich and Fisher. H_2O was >18 MΩ from a Milli-Q water purification system.

Animals and Lethality Test

Animal treatments were performed following "The Guidelines for the Care and Use of Experimental Animals" of National Chiao-Tung University. Four-week-old male BALB/C mice were housed at 22 ± 2 °C with a 12-h light/dark cycle and fed standard rodent chow and water ad libitum. Mice were randomly assigned to experimental groups. Each group consisted of 6 mice. Administration of GNPs was performed by intraperitoneal injection. Animals were sacrificed at the end of experiment by cervical dislocation. The liver, lung, brain, heart, and spleen were isolated, and organ weights of all mice were measured.

Preparation of Gold Nanoparticles

Gold nanoparticles of diameter 3, 5, 8, 12, 17, 37, 50, and 100 nm were synthesized as reported previously [17, 18]. The seed colloids were prepared by adding 1 mL of 0.25 mM $HAuCl_4$ to 90 mL of H_2O and stirred for 1 min at 25 °C. Two milliliters of 38.8 mM sodium citrate were added to the solution and stirred for 1 min, followed by the addition of 0.6 mL of freshly prepared 0.1 M $NaBH_4$ in 38.8 mM sodium citrate. Different diameters of GNPs ranging from 3 to 100 nm were generated by changing the volume of seed colloid added. The solution was stirred for an additional 5–10 min at 0–4 °C. Reaction temperatures and times were adjusted to obtain GNPs of larger size. All synthesized GNPS were characterized by UV absorbance. The size of synthesized GNPs was verified by electron microscopy and atomic force microscopy. GNPs were dialyzed against phosphate-buffered saline (pH 7.4) before injection into the animals.

Enzyme-Linked Immunosorbent Assay (ELISA)

In order to coat wells with GNP as an antigen, each microwell of a 96-well Corning plate was pre-treated with 200 μL of 1 mM 3-aminopropyl-triethoxysilane (APTES) in ethanol at room temperature for 40 min. The activated wells were washed with ethanol twice for 5 min, followed by distilled water for 5 min. GNPs (15 mM, 150 μL) were added to the microwells and incubated for 2 h at room temperature, followed by three Milli-Q water washes and finally with three washes with 0.5% Triton X-100 in PBS. To coat wells with other antigens, 100 μL of antigen was added into microwells and incubated at room temperature for 30 min, followed by three PBS washes. Blocking for non-specific binding was performed by adding 100 μL of 3% bovine serum albumin (BSA) and incubating for 60 min at room temperature, followed by three PBS washes. Binding was performed by adding 100 μL of diluted antiserum into microwells and incubating for 1 h at room temperature, followed by thorough washes. HRP-conjugate anti-mouse IgG, 2,2′-azino-di-(3-ethylbenzthiazoline sulfonic acid) (ABTS) and H_2O_2 were added in sequence to the wells according to the manufacturer's protocol, and the binding efficiency was monitored by measuring absorbance at 405 nm.

Ex Vivo Coherent Anti-Stoke Raman Scattering (CARS) Microscopy

Freshly removed liver and lung tissues were dissected into thin slices of approximately 2 mm in thickness and immersed under PBS in a micro chamber on a glass slide for examination. CARS microscopy was performed with a time constant of 3 ms, a scanning area of 300 × 300 μm, a step size of 1 μm, 300 × 300 pixels, a scanning velocity of 1 μm/ms, and a sampling rate of 80 kHz. Laser power was set at 30 mW for 870 nm and 40 mW for 1064 nm. The wavelengths of the pump and the Stokes lasers (Pump = 870 nm and Stokes = 1064 nm) were tuned to match a Raman shift ($\sim$2100 cm^{-1}) which falls in the so-called "silent region" of the vibrational spectra of cells and tissues. As expected, the CARS images of the "control" did not show appreciable contrast under the non-resonant condition whereas the CARS signals were dramatically

enhanced—appearing as scattered bright spots on the images taken from the GNPs-treated specimens. The enhancement presumably resulted from strong scattering by the GNPs and the large third-order polarizability of the GNPs {Evans, 2005 #90}.

Surface Modification of GNP

The highly immunogenic peptides pFMDV and pH5N1 were designed and synthesized based on viral protein 1 of foot-and-mouth disease virus type O and matrix protein 2 of influenza A virus A/Hong Kong/482/97 H5N1, respectively. The amino acid sequences are NGSSKYGDTSTN NVRGDLQVLAQKAERTLC for pFMDV and MSLLTE VETLTRNGWGCRCSDSSDC for pH5N1. An extra cysteine was added to the C-terminus of each peptide in order to improve binding to the gold surface. BSA and lysozyme were chosen to represent moderately immunogenic antigens. Conjugation of antigen with 17 nm GNPs was performed by titration the antigens into a GNP solution. The titration was monitored by UV absorption at the wavelength appropriate for each peptide to detect aggregation of unsaturated GNP in the presence of 1 M sodium chloride. After reaching the saturation point, the conjugated complexes were purified by centrifugation and resuspended in PBS to final concentration of 0.3 mM.

Results and Discussion

GNPs Ranging from 8 to 37 nm Induced Severe Sickness in Mice

GNPs were synthesized with diameters ranging from 3 to 100 nm according to published procedures [17, 18]. Synthesis of GNPs was monitored by UV absorbance, and the size was examined by electron microscopy (Fig. 1). The purified GNPs had diameters of 3, 5, 8, 17, 12, 37, 50, and 100 nm. They were injected intraperitoneally into BALB/C mice at a dose of 8 mg/kg/week. Mice injected with 3, 5, 50, and 100 nm GNPs behaved normally and survived throughout the experimental period. Mice injected with 8, 17, 12, and 37 nm GNPs exhibited symptoms of toxicity. The treated animals showed fatigue, loss of appetite, change in fur color, and weight loss. There was a dramatic difference in the fur color of GNP-treated mice compared to the normal group, which was usually brownish. The skin underneath had minor rashes, bruising, and hemorrhaging. Starting from day 14, mice injected with 8–37 nm GNPs showed a significantly camel-like back and crooked spine. The majority of mice in these groups died before the end of the fourth week. The median survival time, defined as the length of time when half the mice died, was approximately 21 days for mice injected with 8–37 nm GNPs (Fig. 2).

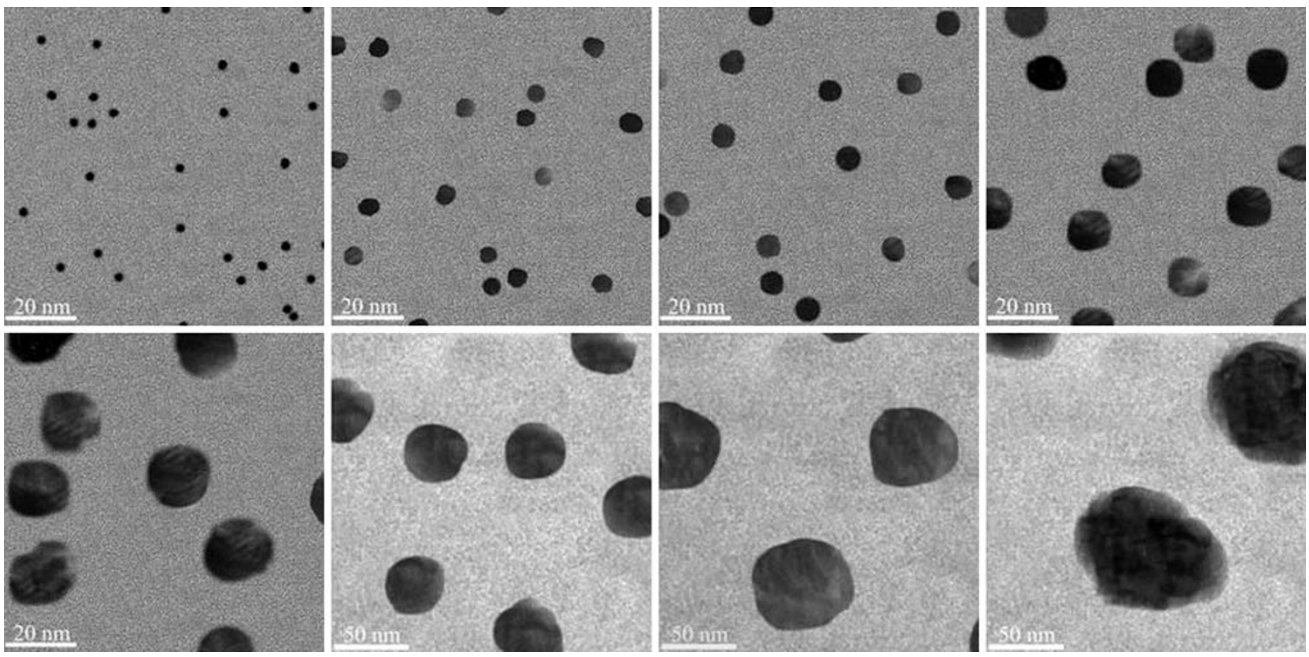

Fig. 1 TEM images for the GNPs synthesized in the current study. GNPs with diameters of 3, 5, 8, 12, 17, 37, 50, and 100 nm were examined under an electron microscope. Scale bars are 20 nm for images of 3, 5, 8, 12, and 17 nm GNPs. Scale bars are 50 nm for images of 37, 50, and 100 nm GNPs

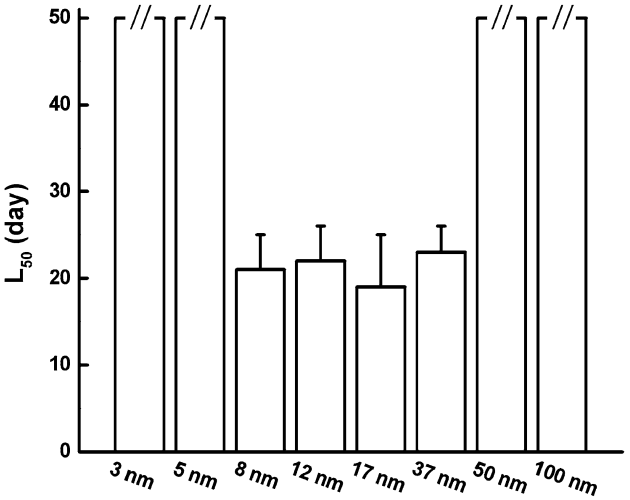

Fig. 2 Average lifespan of mice receiving GNPs with diameters between 8 and 37 nm was shortened to different extents. The average lifespan (L_{50}) was defined as the time beyond which half of the mice died. Mice injected with GNPs outside the lethal range behaved normally. The break marks on the top of bars indicate no death observed during the experimental period

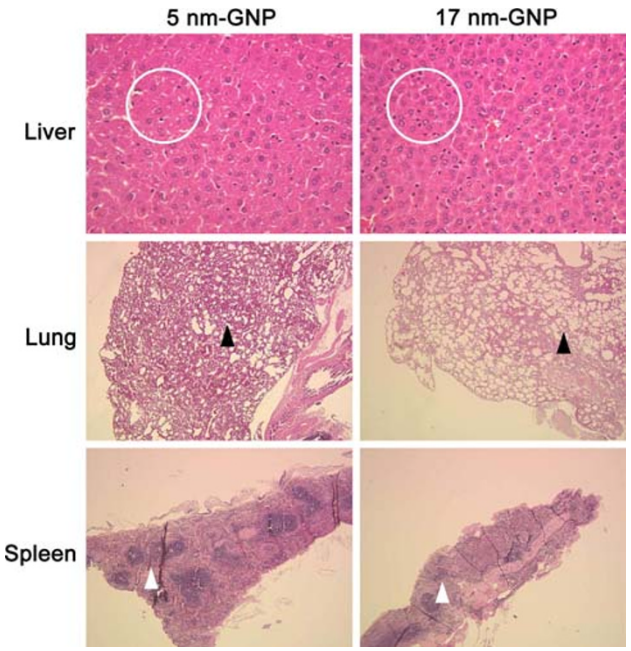

Fig. 3 H&E staining showed GNP-induced abnormality in major organs. (*Top to bottom*) HE staining for liver, lung, and spleen. The *left column* shows tissues from 5 nm GNP-treated animals. The *right column* shows tissues from 17 nm GNP-treated mice

Pathological Abnormalities in GNP-Treated Mice Correlated with the Presence of GNPs in Organs

The acute symptoms and eventual death of mice receiving GNPs indicated that the injected GNPs might damage major organs. In the tissues samples stained with haematoxylin and eosin, the brain, heart, and kidney from 8 to 37 nm GNP-treated mice appeared indistinguishable from tissues in control mice (data not shown). However, the liver, lung, and spleen from 8 to 37 nm GNP-treated mice showed various degrees of abnormality (Fig. 3).

For example, an increase of Kupffer cells (KCs) in the liver was observed in GNP-treated mice. KCs constitute the first macrophage population of the host to come in contact with bacteria, endotoxins, and microbial debris derived from the gastrointestinal tract and transported to the liver. KCs are an important component of the initial and rapid response to potentially dangerous stimuli. Activation of KCs suggested toxic potential for GNPs in this zone [19]. Quantitatively, significant increase of KCs in the liver of 12, 17, and 37 nm GNP-treated mice was observed. Among them, two-fold increase of KCs was observed in 37-nm treated group. GNPs smaller than 8 nm (3 and 5 nm) or larger than 37 nm (50 and 100 nm) did not induce significant KC variations in mouse livers.

Damage in lung tissue structure observed in GNP-treated mice appeared to be similar to that of emphysema. In emphysema, the tiny air sacs (alveoli) in the lungs through which oxygen is absorbed into the bloodstream lose their natural elasticity. Emphysema is a progressive lung condition that leaves sufferers struggling for breath, leading to fatigue, weight loss, and eventually death. Emphysema-like structure was observed in the lung of 8, 12, 17, and 37 nm GNP-treated mice. Other groups did not show aberrant lung structure.

Significant aberration of white pulp was observed in the spleen from GNP-treated mice. The white pulp normally consists of aggregates of lymphoid tissue and is responsible for the immunological function of the spleen. White pulp consisting of splenic nodules appeared diffused in the experimental group. Diffused white pulps were observed in the spleen of 8, 12, 17, and 37 nm GNP-treated mice. Other groups did not show this aberration.

Contaminants of the GNP preparations, such as endotoxins, may have caused damage to organs leading to death. However, all GNPs went through the same synthesis and purification procedure, but GNPs outside the lethal range exhibited no toxic effects on mice. Furthermore, the ELISA using anti-Gram negative endotoxin-IgG showed negative results against all GNPs (Fig. 4). We can therefore exclude the possibility of endotoxin contamination as an explanation for the toxic effects observed in the GNP-treated mice.

It is possible that the abnormalities in the liver, lung, and spleen of GNP-treated mice may have been the consequence of direct contact with the invading GNPs. The injected GNPs may have been transported through blood veins or through diffusion into the liver, lung, and spleen.

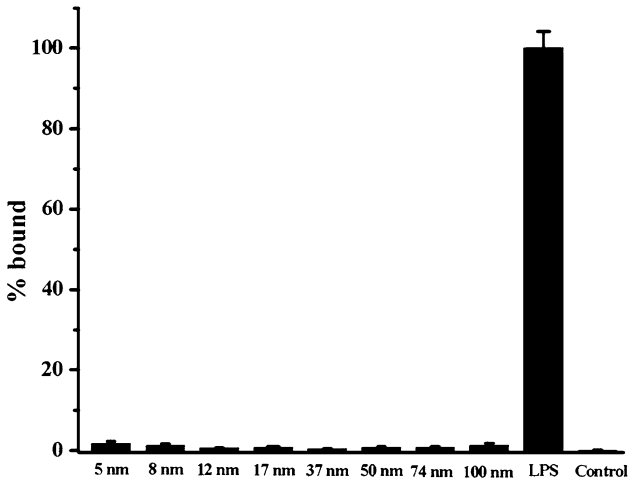

Fig. 4 ELISA of GNPs using anti-endotoxin IgG. ELISA was performed by using anti-endotoxin IgG against various sizes of GNPs synthesized in the lab. Lipopolysaccharide (LPS) served as a positive control, while BSA served as a negative control

To verify the presence of GNPs at the site of abnormality, ex vivo CARS microscopy was performed on the freshly dissected liver tissues [20] (Fig. 5). GNPs are known to enhance the anti-Stoke Raman signal of nearby amino acids. By applying proper controls, CARS microscopy can detect GNPs by measuring this enhancement. Ex vivo diffusion of GNPs into liver tissues was also performed to verify the enhancement of the Raman signal. Localized enhancement of the anti-Stroke Raman signal at an excitation wavelength of 817 nm was observed for livers removed from 8 to 37 nm GNP-treated mice. A significantly weaker signal was observed with livers from 50 nm GNP-treated mice. The Raman signal was totally absent for tissues from 5 nm GNP-treated mice, and tissues from the control group showed no enhancement. The intensity of the Raman signal in the CARS microscopy was proportional to the severity of illness. Our evidence indicates that the dysfunction of major organs is associated with the presence of GNPs at the site of abnormality. Inductively coupled plasma mass spectrometry (ICP-MS) is capable of determining the biodistribution of GNPs with different sizes. Detailed biodistribution profiles could give more useful information to explain the mechanism of toxicity [21–23]. Future experiments will be performed regarding this method.

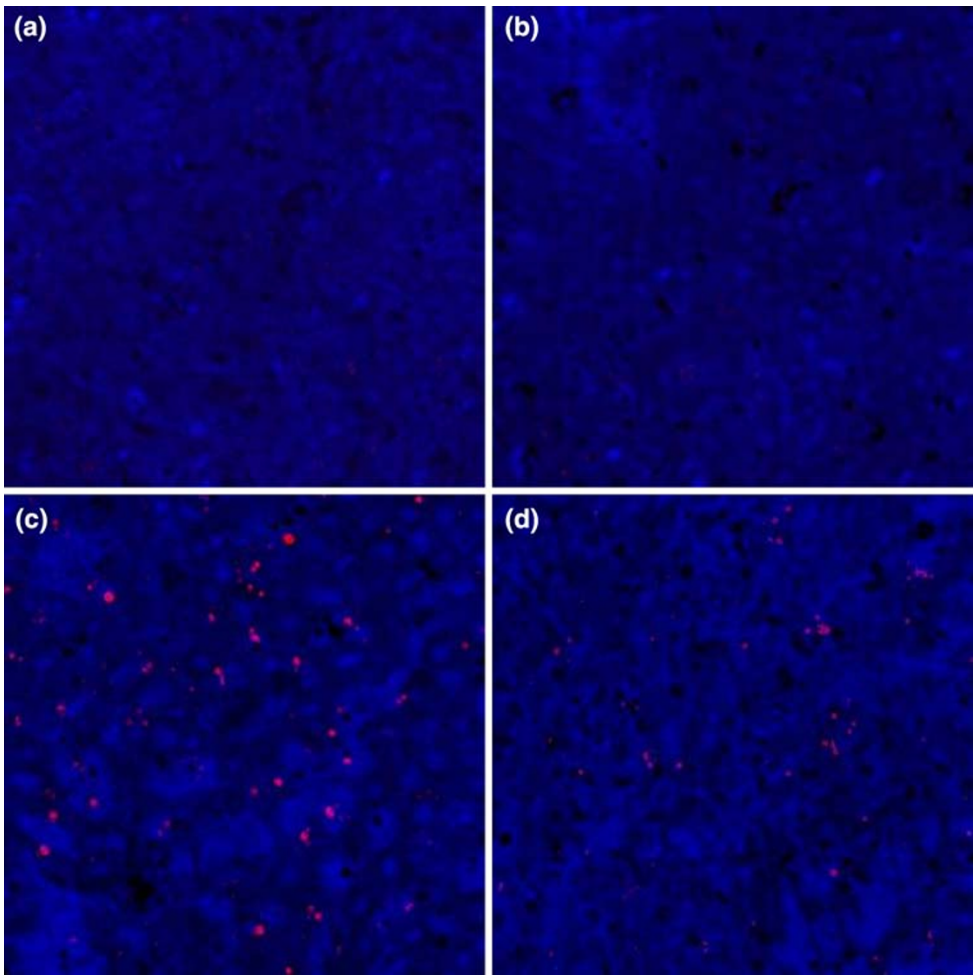

Fig. 5 CARS microscopy of livers isolated from GNP-treated and control mice. The wavelengths of the pump and the Stokes lasers (Pump = 870 nm and Stokes = 1064 nm) were tuned to match a Raman shift ($\sim$2100 cm^{-1}), falling in the so-called "silent region" of the vibrational spectra of cells and tissues. As expected, the CARS images of the "control" did not show appreciable contrast under the non-resonant condition whereas the CARS signals were dramatically enhanced and appeared as scattered bright spots on the images taken from the specimens treated with GNPs. The enhancement presumably resulted from strong scattering from the GNPs and the large third-order polarizability of the GNPs. Enhanced bright spots were observed in neither the control group (**a**) nor the mice injected with 5 nm GNP (**b**). Livers obtained from 17 nm GNP-treated mice showed intense bright spots (**c**). Livers obtained from 50 nm GNP-treated mice showed only a moderate number of spots (**d**)

Enhanced Immunogenicity Ameliorated the Harmful Effect of GNPs

Study of GNP transport using Hela cells indicated that the maximal endocytosis of GNPs occurs when the particles have a diameter of 50 nm [11]. In the current study, injection of 50 nm or larger GNPs, however, did not lead to the death of mice, consistent with the observation that the cell membrane prevents the passage of particles larger than 200 nm. In vivo aggregation of GNPs may have occurred to increase the apparent particle size and lead to the retardation of cellular uptake [24]. We observed that GNPs smaller than 37 nm were lethal to mice, while a further reduction to 5 nm was nontoxic. The alleviation of the lethal effect for 3 and 5 nm GNPs remains to be explored.

It is possible that the difference in lethality may reflect a difference in cellular toxicity. A colorimetric methyl-thiazol-tetrazolium (MTT) assay was performed to measure the cytotoxicity of GNPs in cultured Hela cells. The viability of cells exceeded 80% at the highest concentration of GNP (0.4 mM), indicating that regardless of their size, all GNPs were essentially non-toxic to Hela cells (Fig. 6). The inconsistency of cytotoxicity and lethality indicated that factors other than cytotoxicity may be involved in the amelioration of the lethal effect for 3 and 5 nm GNPs.

We have previously shown that serum obtained from mice injecting with 5 nm GNPs showed specific binding activity to GNPs, while serum from mice immunized with larger-sized GNPs showed only background binding [16]. This differential immune response of mice to different sizes of GNPs indicates that the scavenging activity of the immune system may play a role in the size-dependent lethality of GNPs. To test this hypothesis, surface modification of 17 nm GNPs was carried out so that they would display a spectrum of epitopes. The highly immunogenic peptides pFMDV and pH5N1 were designed and synthesized based on viral protein 1 of foot-and-mouth disease virus type O and matrix protein 2 of influenza A virus (A/Hong Kong/482/97(H5N1)), respectively. BSA and lysozyme were selected to represent moderately immunogenic antigens. As a positive control, mice were injected with unmodified 17 nm GNPs. Injection of surface-modified GNPs caused a spectrum of lethality in mice (Fig. 7). pFMDV and pH5N1 conjugation extended the average lifespan from 21 days to more than 50 days. Lysozyme modification elongated the lifespan to 27.5 days, while BSA modification caused elongation to 22.3 days. The titer of antigen binding activity of sera was verified by ELISA (Fig. 7). Sera obtained from groups injected with pFMDV and pH5N1-conjugated 17 nm GNPs exhibited the highest titer. Lysozyme- and BSA-coated GNPs induced moderate titers. The ability of coated-GNPs to reduce the lethal effect was closely associated with their ability to induce an antibody response. In rodents, quantum dots with final hydrodynamic diameter <5.5 nm resulted in rapid and efficient urinary excretion and elimination from the body [25]. Urinary secretion may play an important role to remove GNPs under 5 nm in our model.

GNPs caused a range of lethality when injected into mice. GNPs larger than 50 nm were nontoxic to mice, which can be interpreted as a diffusion-restricted region. The nontoxic effect of GNPs smaller than 5 nm can be

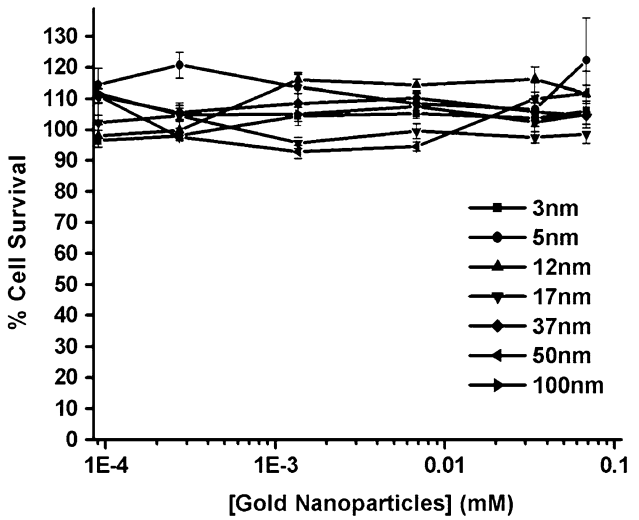

Fig. 6 MTT assay to obtain LC_{50} for different sizes of GNPs using Hela cells as a model system. After seeding and proper attachment, the Hela cells were treated with 5, 8, 12, and 17 nm GNPs at the concentrations, indicated on the horizontal axis. The percentage of survival was plotted against GNPs concentration

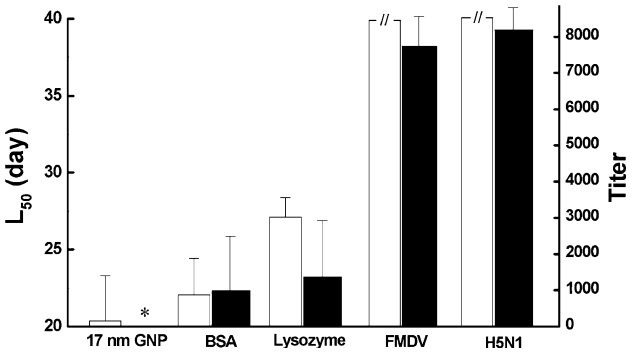

Fig. 7 The lethality and immunogenicity of surface-modified 17 nm GNPs. Average lifespans of mice injected with modified 17 nm GNPs are shown in empty columns. Each experimental group received GNP conjugated with BSA, lysozyme, pFMDV, or pH5N1. Unmodified GNPs served as a positive control (17 nm GNP). Titers of antiserum withdrawn from GNP-injected mice against corresponding antigens are shown in filled columns. pH5N1- and pFMDV-coated GNPs induced the highest titer in mouse serum; BSA- and lysozyme-coated GNPs induced a moderate titer; and unmodified GNPs did not induce an antibody response in mice (*)

explained by the increase in antibody response that enhanced the scavenging effect. Apparently, the lethal effect is due to the inability of GNPs to stimulate a strong immune response, which allows them to diffuse freely into cells.

Conclusions

GNPs may exhibit low cellular toxicity in cultured cells. Here, we show that given a sufficient dose, the invasion of seemingly nontoxic GNPs can have a lethal effect on mice. Although the exact mechanism responsible for this lethal effect is not clear at present, studies have suggested the presence of GNPs at the diseased sites. While GNPs have been widely used for targeting and imaging in drug delivery, the toxicity due to their nanometer dimensions must be a major concern. In addition to emphasizing this toxicity, our study also provides an important basis for studying the environmental toxicity of fine particles.

Acknowledgments This study was supported in part by the National Science Council in Taiwan (grant NSC94-2320-B-009-003) and the Bureau of Animal and Plant Health Inspection and Quarantine Council of Agriculture in Taiwan (grants 95AS-13.3.1-BQ-B1 and 95AS-13.3.1-BQ-B6).

References

1. P.J. Borm, D. Muller-Schulte, Nanomed **1**, 235 (2006). doi:10.2217/17435889.1.2.235
2. P.J. Borm, D. Robbins, S. Haubold, T. Kuhlbusch, H. Fissan, K. Donaldson, R. Schins, V. Stone, W. Kreyling, J. Lademann, J. Krutmann, D. Warheit, E. Oberdorster, Part. Fibre Toxicol. **3**, 11 (2006). doi:10.1186/1743-8977-3-11
3. K.A. Guzman, M.R. Taylor, J.F. Banfield, Environ. Sci. Technol. **40**, 1401 (2006). doi:10.1021/es0515708
4. J.C. Carrero-Sanchez, A.L. Elias, R. Mancilla, G. Arrellin, H. Terrones, J.P. Laclette, M. Terrones, Nano Lett. **6**, 1609 (2006). doi:10.1021/nl060548p
5. S. Fiorito, A. Serafino, F. Andreola, A. Togna, G. Togna, J. Nanosci. Nanotechnol. **6**, 591 (2006). doi:10.1166/jnn.2006.125
6. S. Zhu, E. Oberdorster, M.L. Haasch, Mar. Environ. Res. **62**(Suppl), S5 (2006). doi:10.1016/j.marenvres.2006.04.059
7. G. Federici, B.J. Shaw, R.D. Handy, Aquat. Toxicol. **84**, 415 (2007). doi:10.1016/j.aquatox.2007.07.009
8. J. Park, S. Bauer, K. Von der Mark, P. Schmuki, Nano Lett. **7**, 1686 (2007). doi:10.1021/nl070678d
9. J.R. Gurr, A.S. Wang, C.H. Chen, K.Y. Jan, Toxicology **213**, 66 (2005). doi:10.1016/j.tox.2005.05.007
10. B.D. Chithrani, W.C. Chan, Nano Lett. **7**, 1542 (2007). doi:10.1021/nl070363y
11. B.D. Chithrani, A.A. Ghazani, W.C. Chan, Nano Lett. **6**, 662 (2006). doi:10.1021/nl052396o
12. M.L. Becker, L.O. Bailey, K.L. Wooley, Bioconjug. Chem. **15**, 710 (2004). doi:10.1021/bc049945m
13. E.E. Connor, J. Mwamuka, A. Gole, C.J. Murphy, M.D. Wyatt, Small **1**, 325 (2005). doi:10.1002/smll.200400093
14. T.S. Hauck, A.A. Ghazani, W.C. Chan, Small **4**, 153 (2007). doi:10.1002/smll.200700217
15. G.F. Paciotti, L. Myer, D. Weinreich, D. Goia, N. Pavel, R.E. McLaughlin, L. Tamarkin, Drug Deliv. **11**, 169 (2004). doi:10.1080/10717540490433895
16. G.S. Huang, Y.S. Chen, H.W. Yeh, Nano Lett. **6**, 2467 (2006). doi:10.1021/nl061598x
17. K.R. Brown, D.G. Walter, M.J. Natan, Chem. Mater. **12**, 306 (2000). doi:10.1021/cm980065p
18. F.K. Liu, C.J. Ker, Y.C. Chang, F.H. Ko, T.C. Chu, B.T. Dai, Jpn. J. Appl. Phys. **42**, 4152 (2003). doi:10.1143/JJAP.42.4152
19. E. Sadauskas, H. Wallin, M. Stoltenberg, U. Vogel, P. Doering, A. Larsen, G. Danscher, Part. Fibre Toxicol. **4**, 10 (2007). doi:10.1186/1743-8977-4-10
20. C.L. Evans, E.O. Potma, M. Puoris'haag, D. Cote, C.P. Lin, X.S. Xie, Proc. Natl. Acad. Sci. USA **102**, 16807 (2005). doi:10.1073/pnas.0508282102
21. G. Sonavane, K. Tomoda, K. Makino, Colloids Surf. B Biointerfaces **66**, 274 (2008). doi:10.1016/j.colsurfb.2008.07.004
22. C.R. Patra, R. Bhattacharya, E. Wang, A. Katarya, J.S. Lau, S. Dutta, M. Muders, S. Wang, S.A. Buhrow, S.L. Safgren, M.J. Yaszemski, J.M. Reid, M.M. Ames, P. Mukherjee, D. Mukhopadhyay, Cancer Res. **68**, 1970 (2008). doi:10.1158/0008-5472.CAN-07-6102
23. W.H. De Jong, W.I. Hagens, P. Krystek, M.C. Burger, A.J.A.M. Sips, R.E. Geertsma, Biomaterials **29**, 1912 (2008). doi:10.1016/j.biomaterials.2007.12.037
24. B.M. Rothen-Rutishauser, S. Schurch, B. Haenni, N. Kapp, P. Gehr, Environ. Sci. Technol. **40**, 4353 (2006). doi:10.1021/es0522635
25. H.S. Choi, W. Liu, P. Misra, E. Tanaka, J.P. Zimmer, B. Itty Ipe, M.G. Bawendi, J.V. Frangioni, Nat. Biotechnol. **25**, 1165 (2007). doi:10.1038/nbt1340